

Magnetic Structures of an Iron–Gadolinium Multilayer at Low Temperatures

Nobuyoshi HOSOITO¹, Hiroo HASHIZUME^{*}, Naoki ISHIMATSU², In-Tae BAE,[†] George SRAJER³, Jonathan C. LANG³, Chitra K. VENKATARAMAN³ and Christie S. NELSON³

Research and Education Center for Materials Science, Nara Institute of Science and Technology, Ikoma 630-0101, Japan

¹*Institute for Chemical Research, Kyoto University, Uji 611-0011, Japan*

²*Department of Physical Science, Graduate School of Science, Hiroshima University, Higashi-Hiroshima 739-8526, Japan*

³*Advanced Photon Source, Argonne National Laboratory, Argonne IL 60439, U.S.A.*

(Received October 25, 2001; accepted for publication December 13, 2001)

Low-temperature magnetic structures of an [Fe/Gd]₁₅ multilayer are determined using the resonant X-ray magnetic scattering technique at a synchrotron source. The difference intensities of specular Bragg reflections observed by flipping the helicity of circularly polarized probing X-rays of energy close to the L₃ absorption edge of Gd show that the multilayer is in the Gd-aligned state with the magnetic moments of the Gd layers oriented parallel to the applied in-plane field at $H = 0.5$ kOe, $T = 10$ K. This transforms into the twisted state with canted Gd moments by raising field strength H and/or temperature T . In the twisted state, the Gd moments at the interfaces and the core of the Gd layers show distinctive canting angles. Temperature and field-dependent in-plane rotations of local Gd moments have been visualized. [DOI: 10.1143/JJAP.41.1331]

KEYWORDS: magnetic multilayer, spin arrangement, rare-earth film, exchange interaction, resonant X-ray magnetic reflectometry, synchrotron radiation

1. Introduction

Fe/Gd multilayers are thin films of $3d-4f$ systems showing intriguing magnetic structures that depend on temperature T and the strength H of an externally applied field. Camley and co-workers calculated (H, T) phase diagrams for Fe/Gd, which show the so-called Fe-aligned state, twisted state and Gd-aligned state.^{1–3)} In the aligned states, the magnetic moments of Fe and Gd layers line up with the applied in-plane field, whereas they are canted from the field direction in the twisted states. The three states originate in the significantly different magnetic properties of Fe and Gd, and the phase change in idealized systems is understood in terms of the competition between the Zeeman energy and the exchange interaction energy.^{1–3)} The structural features of the three states were evidenced in experiments using the magnetization measurement,^{4,5)} magnetoresistance,^{4,6)} Mössbauer spectroscopy,⁷⁾ neutron diffraction,^{8,9)} and X-ray magnetic circular dichroism (XMCD)^{10–12)} techniques. In the previous paper,¹³⁾ we showed that spin configurations in real multilayers are much more complicated than originally conceived. We used the resonant X-ray magnetic scattering (RXMS) technique, of which element specificity allowed us to separately determine the Fe and Gd structures in an [Fe(3.5 nm)/Gd(5.4 nm)]₁₅ multilayer. The spin structures in the Gd layers are remarkably nonuniform along the out-of-plane direction. In an in-plane field of 2.4 kOe, Gd sublayers at the Fe interfaces are almost completely magnetized in the entire temperature range studied ($140 \text{ K} \leq T \leq 300 \text{ K}$), whereas the core sublayers show spontaneous magnetizations proportional to $1 - (T/T_c)$ with $T_c = 214 \text{ K}$, suggesting a reduced Curie temperature for the thin Gd layers ($T_c = 292 \text{ K}$ for bulk Gd). The magnetic structure of this sample is Fe-aligned for $180 \text{ K} \leq T \leq 300 \text{ K}$ and twisted for $140 \text{ K} \leq T \leq 160 \text{ K}$. We observed highly nonuniform canting angles of sublayer

Gd moments along the out-of-plane direction in the twisted state. The interface moments appear to be constrained by the antiferromagnetic exchange interaction with the Fe moments, whereas the core moments are freer to rotate in the in-plane direction. A simple picture of uniformly twisted moments does not apply to the twisted states of real Fe/Gd multilayers.

In this study, we extend the investigation to lower temperatures. The Gd-aligned state occurs in a low external magnetic field at $T < T_{\text{comp}}$, the compensation temperature, where the total Gd moment becomes greater than the total Fe moment and parallel Gd moments are favored because of the low Zeeman energy.^{1–3)} At low temperatures, Gd shows a non-negligible magnetic anisotropy due to crystal-field effects and this complicates the magnetic structures of the Gd-aligned state in real systems. The energy calculation schemes formulated by Camley and co-workers^{1–3)} do not take into account the anisotropy energy. When this energy occupies a significant fraction of the total magnetic energy of the system, there is no distinct transition between the Gd-aligned and twisted states on an atomic scale. The X-ray magnetic scattering data to be discussed in this paper have been presented in ref. 14, with a brief description of the experiment. We give a more complete description in this paper (§2) and analyze the data to discuss the magnetic structures of Fe/Gd at low temperatures (§3 and §4). Section 5 contains the conclusion.

2. Experiment and Results

The sample [Fe/Gd]₁₅ multilayer film was grown in the same ultrahigh-vacuum molecular-beam-epitaxy chamber ($3 \times 10^{-7} \text{ Pa}$) as used for the previous sample.¹³⁾ Fe and Gd were deposited on a Si(111) substrate at room temperature at the rate of $1.2\text{--}1.8 \text{ nm min}^{-1}$. The beam shutters were controlled to alternately grow 3.5-nm-thick Fe and 5.0-nm-thick Gd layers. The first grown layer is Gd and an Fe layer terminates the multilayer. The same multilayer was grown on a Kapton film for magnetization measurements in the same deposition run as the X-ray sample. An X-ray diffractometer scan on the prepared multilayer showed a broad *hcp* Gd 0002 peak, indicative of a polycrystalline

^{*}Author to whom correspondence should be addressed. E-mail: hhashizu@ms.aist-nara.ac.jp

[†]Present address: Department of Materials Science and Engineering, Graduate School of Engineering, Osaka University, Yamadaoka, Suita 565-0871, Japan.

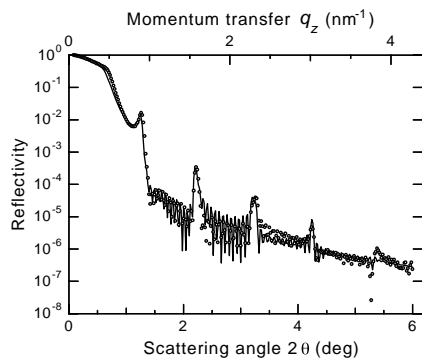


Fig. 1. Charge specular reflectivity profile of the $[\text{Fe/Gd}]_{15}$ sample recorded with $\text{Cu K}\alpha$ X-rays (circles). Solid line shows a fit.

structure of the Gd layers. This conforms to our expectation that the structures of Fe and rare-earth films change from amorphous to crystalline when the deposited thickness exceeds $\approx 2\text{ nm}$. This is consistent with the observation made by Sajieddine *et al.*,⁷⁾ as well.

Figure 1 shows a charge X-ray specular reflectivity profile for the sample, recorded at a $\text{Cu K}\alpha$ source. The four pronounced peaks are superlattice Bragg reflections at scattering angles $2\theta = 2\sin^{-1}(n\lambda/2\Lambda)$ ($n = 1-4$), where Λ is the multilayer spacing and λ is the X-ray wavelength. The profile is well explained by the chemical structure parameters listed in Table I. We assumed uniform electron densities for the Fe and Gd layers with abrupt, rough interfaces between them. Possible oxidation of the top Fe layer was taken into account by postulating a chemical composition of 50% Fe and 50% O for the surface oxide layer. A least-squares profile fit gave $t_{\text{Fe}} = 3.53\text{ nm}$ and $t_{\text{Gd}} = 4.85\text{ nm}$ for the mean thicknesses of the Fe and Gd layers, with densities $\rho_{\text{Fe}}^* = 0.864$ and $\rho_{\text{Gd}}^* = 0.942$ relative to bulk *bcc* Fe and *hcp* Gd, respectively (Table I). The Gd layers have a slightly smaller thickness than in the previous sample, whereas the Fe layers are of similar thickness.¹³⁾ The oxidation of the sample is likely to have stopped at about one-half the thickness of the top Fe layer. This is consistent with the observation by Shinjo *et al.*,¹⁵⁾ showing that a 1–2 nm surface layer is oxidized when an Fe film is exposed to air and that the oxidation does not proceed into deeper layers when the film is placed in a dry environment. The root-mean-square roughness of the Fe/Gd and Gd/Fe interfaces, which were assumed to be equally rough, is $\sigma_{\text{Fe/Gd}} = \sigma_{\text{Gd/Fe}} = 0.67\text{ nm}$. The air/oxide and oxide/Fe interfaces are much rougher. The good agreement of the experimental and calculated specular profiles in Fig. 1 is evidence that the postulated model adequately describes the chemical structure of the sample.

RXMS data were collected at the Gd L_3 absorption edge on the 1-ID beamline of Advanced Photon Source, Argonne National Laboratory, U.S.A. The $[\text{Fe/Gd}]_{15}$ multilayer sample, $4 \times 4 \times 0.6\text{ mm}$ in size, was placed in the air gap of a permanent magnet. Spacer plates introduced between the permanent magnet and the iron pole pieces allowed fields of 0.5 and 5 kOe to be applied parallel to the sample surface. The assembly was placed inside a Displex-type closed-helium-cycle cryostat, which was mounted on a Huber four-circle goniometer (Fig. 2). Using the vertical dispersion

Table I. Chemical structure parameters for the $[\text{Fe/Gd}]_{15}$ multilayer determined by least-squares fits of the X-ray reflectivity data. See text for the symbols. The figures in the parentheses indicate the expected standard deviations in units of the least-significant digit given.

$\sigma_{\text{air/oxide}}$	1.73 (5) nm
t_{oxide}	3.80 (10) nm
$\sigma_{\text{oxide/Fe}}$	1.73 (5) nm
$t_{\text{top Fe}}$	1.81 (9) nm
t_{Fe}	3.53 (0) nm
t_{Gd}	4.85 (0) nm
$\sigma_{\text{Fe/Gd}}, \sigma_{\text{Gd/Fe}}$	0.67 (2) nm
$\sigma_{\text{Gd/Si}}^{\text{a)}$	0.22 (2) nm
$\rho_{\text{Fe}}^{\text{b)}$	0.864 (7)
$\rho_{\text{Gd}}^{\text{b)}$	0.942(10)

a) r.m.s roughness at the bottom Gd-layer/substrate Si interface.

b) Densities relative to bulk materials.

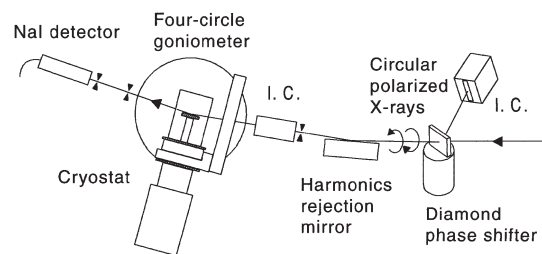


Fig. 2. The setup used to collect the resonant X-ray magnetic scattering data (side view). The diamond phase shifter oscillates on a 45° -inclined rotation axis to convert the plane polarized synchrotron X-rays into circular polarized light of flipping helicity. The harmonics rejection mirror eliminates the $\lambda/3$ component of the X-ray beam monochromatized using a cryogenically cooled $\text{Si}(111)$ double-crystal monochromator (not shown). The permanent magnet placed inside the cryostat is not shown. Intensity measurements are performed for fixed X-ray counts on the monitor ion chamber (I.C.) placed behind the harmonics rejection mirror.

geometry, we scanned the reciprocal space along the specular rod while a 0.4-mm-thick diamond quarter-wavelength plate oscillated across the 111 Bragg position to flip the helicity of the circularly polarized transmitted beam between $+1$ and -1 . The degree of circular polarization of the beam is estimated to be $P_c \approx 0.92$. More than 10^6 photons were counted at each scan point around the four superlattice Bragg peaks of the $[\text{Fe/Gd}]_{15}$ sample for each polarization state of the probing X-rays. $I^+(q_z)$ data and $I^-(q_z)$ data were thus obtained, where I^+ and I^- are the specular intensities measured with X-rays of helicity of the sign same as and opposite to the sign of the in-plane field applied on the sample, respectively.¹⁶⁾ For instance, I^+ is the scattering intensity measured with $+(−)$ field and probing X-rays of $+1(−1)$ helicity. Refer to ref. 13 for the definition of the field sign. In an analogy to neutron scattering, one may call the X-ray helicity the photon spin, which interacts with electron spins, but this alias is misleading. It is the orbital moment of the probed electrons that the X-ray helicity interacts with and it is through the spin-orbit interaction that $I^+ - I^-$ becomes spin sensitive. q_z is the out-of-plane momentum transfer, which equals $4\pi \sin \theta / \lambda$ in the specular reflection geometry. We do not analyze the

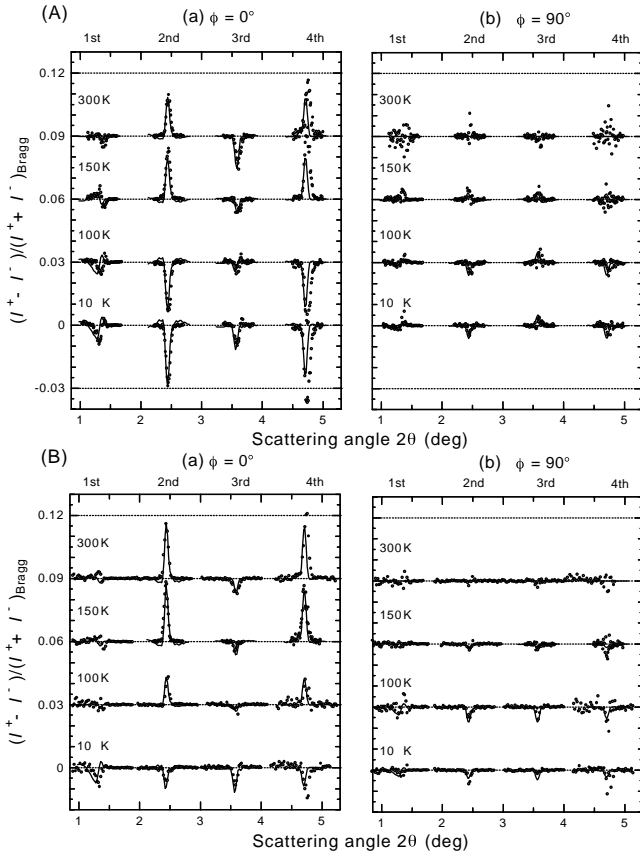


Fig. 3. Temperature and field-strength variation of the first, second, third and fourth-order difference superlattice Bragg peaks observed from the $[\text{Fe}/\text{Gd}]_{15}$ multilayer sample, normalized by the X-ray counts of the sum intensities at the individual Bragg peaks. X-ray energy: 7244.5 eV. (A) For an applied in-plane field strength of 0.5 kOe and (B) for 5 kOe. (a) For the $\phi = 0^\circ$ configuration and (b) for the $\phi = 90^\circ$ configuration. Open circles: observed, solid line: simulated.

polarization of scattered X-rays. In this case, the difference intensity $I^+(q_z) - I^-(q_z)$ is only sensitive to the parallel magnetization of the resonating Gd layers, namely, the component of the Gd magnetic moment parallel to the dispersion plane defined by \mathbf{k} and \mathbf{k}' , the wave vectors of the incoming and outgoing X-rays.¹⁷⁾ Nonresonant magnetic scattering from the Fe layers is much weaker than the resonance enhanced Gd scattering and can be ignored. Specular scans were carried out in two azimuthal orientations of the sample, $\phi = 0^\circ$ and 90° (see Fig. 3 of ref. 13), realized by rotating the whole cryostat on the goniometer around the surface normal of the sample. In the $\phi = 0^\circ$ and 90° configurations, the applied field is parallel and perpendicular to the dispersion plane, and hence the in-line and perpendicular components of the in-plane Gd magnetization are probed, respectively.

We followed the procedure described in ref. 13 to fix the X-ray energy at 7244.5 eV, 1.0 eV below the peak of the X-ray magnetic circular dichroic (XMCD) absorption spectrum at the Gd L_3 edge. The XMCD data were used to evaluate the real and imaginary parts of the resonant magnetic scattering factors of Gd,¹³⁾ g'_m and g''_m : $g'_m = -0.0624$ and $g''_m = 0.108$ in electron units. The anomalous dispersion corrections for the Gd charge scattering factor, $f'_c(\text{Gd})$ and $f''_c(\text{Gd})$, were derived from the measured nonmagnetic

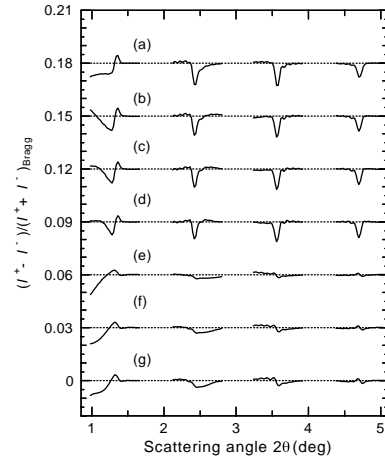


Fig. 4. Effects of rotated magnetic moments in zero (a), one (b, e), two (c, f) and three (d, g) surface Gd layers of the $[\text{Fe}/\text{Gd}]_{15}$ multilayer in the Gd-aligned state. (a)–(d) for the $\phi = 0^\circ$ configuration and (e)–(g) for the $\phi = 90^\circ$ configuration. $(m_{\parallel,1}, m_{\parallel,2}, m_{\parallel,3}, m_{\parallel,4}, \dots, m_{\parallel,15}) = (1, 1, 1, 1, \dots, 1)$ for (a), $(0, 1, 1, 1, \dots, 1)$ for (b), $(0, 1/2, 1, 1, \dots, 1)$ for (c), and $(0, 1/3, 2/3, 1, \dots, 1)$ for (d); $(m_{\perp,1}, m_{\perp,2}, m_{\perp,3}, m_{\perp,4}, \dots, m_{\perp,15}) = (1, 0, 0, 0, \dots, 0)$ for (e), $(1, \sqrt{3}/2, 0, 0, \dots, 0)$ for (f), and $(1, \sqrt{8}/3, \sqrt{5}/3, 0, \dots, 0)$ for (g). Compare with the observed Bragg peak profiles for $T = 10$ K in Fig. 3B.

absorption curve of a Gd foil. For further details of the experiment, readers are encouraged to refer to the previous paper.¹³⁾

Figure 3 shows the difference specular intensities divided by the sum intensities at the individual Bragg peaks, $(I^+ - I^-)/(I^+ + I^-)_{\text{Bragg}}$, for the first, second, third, and fourth-order superlattice Bragg reflections ($q_z = 2n\pi/\Lambda$, $n = 1-4$), measured at temperatures $T = 300, 150, 100$, and 10 K and applied in-plane fields $H = 0.5$ (Fig. 3A) and 5 kOe (Fig. 3B). These are the same data as presented in Figs. 4 and 5 of ref. 14. Difference intensity $I^+ - I^-$ represents the interference of the resonant magnetic scattering from the Gd layers and the charge scattering from the entire multilayer, whereas sum intensity $I^+ + I^-$ is due to the Thomson charge scattering from the entire multilayer.¹⁸⁾ Flipping ratio $R = (I^+ - I^-)/(I^+ + I^-)$ may be taken as the structure amplitude of the magnetic scattering divided by that of the charge scattering. In the left panel of Fig. 3(a) ($\phi = 0^\circ$), the X-ray dispersion plane is parallel to the in-plane field, while it is perpendicular in the right panel of Fig. 3(b) ($\phi = 90^\circ$). We checked the invariability of the $I^+ - I^-$ signal on a 180° rotation of the applied-field direction around the sample surface normal. $I^+ - I^-$ remained unchanged within 10% by $\phi = 0^\circ \rightarrow 180^\circ$ and by $\phi = 90^\circ \rightarrow 270^\circ$.¹⁹⁾ This ensures a proper measurement of the magnetic-charge interference scattering. In failed experiments, I^+ and/or I^- are often biased and $I^+ - I^-$ does not show the expected invariability upon a reversal of the field direction.²⁰⁾ The scattering profiles in Fig. 3 are featured by the even-order Bragg peaks changing the signs at certain temperatures T in the $\phi = 0^\circ$ configuration [Figs. 3A(a) and 3B(a)]. This indicates significant changes take place in the in-line magnetic structures of the Gd layers at these temperatures. Another feature noted is the all-negative Bragg peaks observed in the $\phi = 90^\circ$ configuration at $T \leq 100$ K, $H = 5$ kOe [Fig. 3B(b)]. Taken together with

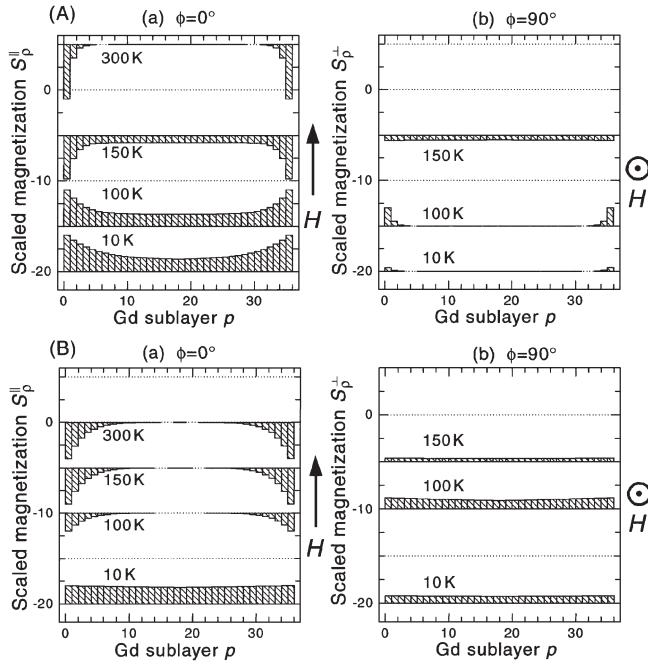


Fig. 5. Model magnetization depth profiles for the Gd layers. A 4.85-nm-thick Gd layer is divided into 36 sublayers p to fit the normalized difference Bragg peak profiles shown in Fig. 3. (A) For applied in-plane field strength $H = 0.5$ kOe and (B) for 5 kOe. (a) For the $\phi = 0^\circ$ configuration and (b) for the $\phi = 90^\circ$ configuration. The applied field H is directed upward in (a) and out of the page in (b) as indicated in the figure.

the finite signals in the $\phi = 0^\circ$ configuration [Fig. 3B(a)], this immediately indicates twisted Gd moments even at $T = 10$ K, as pointed out in ref. 14.

3. Magnetic Structures of the Gd Layers at Low Temperatures

We proposed in the previous paper¹³⁾ a formula to calculate the magnetic specular reflectivity of multilayers for circularly polarized probing X-rays. The formula, including dynamical effects and the polarization mixing, allows us to calculate $(I^+ - I^-)/(I^+ + I^-)_{\text{Bragg}}$ as a function of q_z for a given model $\mathbf{M}(Z)$, where $\mathbf{M}(Z)$ is the depth profile of in-plane magnetization for the sample under investigation. Only the resonating atoms, Gd in the present case, are pertinent to $\mathbf{M}(Z)$. Independent fits to the $(I^+ - I^-)/(I^+ + I^-)_{\text{Bragg}}$ data collected in the $\phi = 0^\circ$ and 90° configurations determine $M_{\parallel}(Z)$ and $M_{\perp}(Z)$ respectively, where M_{\parallel} and M_{\perp} are the components of \mathbf{M} in line with and perpendicular to the applied in-plane field, respectively. The ratio of the two components, $M_{\perp}(Z)/M_{\parallel}(Z)$, gives in-plane twist angle $\psi(Z)$ of local moment \mathbf{M} at depth Z .

In an attempt to fit the data of Fig. 3, we first tested simple models assuming an identical magnetization depth profile $\mathbf{m}(z)$ for the fifteen Gd layers in the sample, where z is the out-of-plane coordinate within a Gd layer. Namely, we assumed $\mathbf{m}_j(z) = \mathbf{m}(z)$ for $j = 1-15$, where $\mathbf{m}_j(z)$ is the magnetization depth profile for the j th Gd layer and $\mathbf{M}(Z) = \sum_j \mathbf{m}_j(z + Z_{0j})$. Note that $\mathbf{m}_j(z)$ is the local in-plane magnetization vector at depth z . $m_{\parallel,j}(z)$ and $m_{\perp,j}(z)$ are its components parallel and perpendicular to the applied-field direction, respectively. Figure 4(a) shows the $(I^+ - I^-)/(I^+ + I^-)_{\text{Bragg}}$ profile calculated from one of the models that

fits quite well the data for $T = 10$ K in Fig. 3B(a) ($\phi = 0^\circ$, $H = 5$ kOe; the bottom-left profile), except on the low- 2θ flank of the first Bragg peak, where there is a significant discrepancy. While the observed signal falls to zero and swings somewhat to the positive side at $2\theta \approx 1^\circ$ [$q_z \approx 0.6 \text{ nm}^{-1}$ in Fig. 3B(a)], the calculated profile shows a negative plateau [Fig. 4(a)]. This plateau is suppressed in models where a few Gd layers close to the multilayer surface have smaller in-line magnetizations m_{\parallel} 's than the deeper layers. Profiles (b), (c) and (d) are calculated assuming $(m_{\parallel,1}, m_{\parallel,2}, m_{\parallel,3}, m_{\parallel,4}, \dots, m_{\parallel,15}) = (0, 1, 1, 1, \dots, 1)$, $(0, 1/2, 1, 1, \dots, 1)$ and $(0, 1/3, 2/3, 1, \dots, 1)$, respectively. In these models, the near-surface Gd layers contribute fully to $I^+ + I^-$, but make no or smaller contributions to $I^+ - I^-$ of the $\phi = 0^\circ$ configuration than the Gd layers located deep in the multilayer. A magnetically dead surface layer suppresses $I^+ - I^-$ more strongly at lower 2θ because of the strong X-ray absorption. A comparison of the profiles in Fig. 4 with the data in Fig. 3B(a) ($T = 10$ K) indicates that the $(0, 1/2, 1, 1, \dots, 1)$ model [profile (c)] gives a slightly better fit than the other two. Two possible origins of the reduced in-line magnetizations in the near-surface Gd layers are (i) in-plane rotation of the moments away from the in-line orientation and (ii) demagnetization due to the surface oxidation. If (i) is the case, we have $m_{\perp,j} = [1 - (m_{\parallel,j})^2]^{1/2}$ and the corresponding perpendicular magnetizations are $(m_{\perp,1}, m_{\perp,2}, m_{\perp,3}, m_{\perp,4}, \dots, m_{\perp,15}) = (1, 0, 0, 0, \dots, 0)$, $(1, \sqrt{3}/2, 0, 0, \dots, 0)$ and $(1, \sqrt{8}/3, \sqrt{5}/3, 0, \dots, 0)$, which give scattering profiles (e), (f) and (g), respectively (Fig. 4). All these show negative falloffs at $2\theta \approx 1^\circ$, which are absent in the data in Fig. 3B(b) for $H = 5$ kOe, $T = 10$ K ($\phi = 90^\circ$; the bottom-right profile). It is thus necessary to assume reduced perpendicular magnetizations in near-surface Gd layers to account for the specular reflectivity profiles observed in the $\phi = 90^\circ$ configuration. This makes (i) unlikely and favors (ii) for the origin of the reduced in-line magnetizations.

The solid lines in Fig. 3 show the Bragg-peak profiles calculated from the model assuming $(|\mathbf{m}_1|, |\mathbf{m}_2|, |\mathbf{m}_3|, \dots, |\mathbf{m}_{15}|) = (0, 1/2, 1, \dots, 1)$, which features the nonmagnetic outermost Gd layer and the half-demagnetized second layer. Figure 5 shows the magnetization profiles, $m_{\parallel}(z)$ and $m_{\perp}(z)$, used to calculate the solid lines in Fig. 3. The calculation used the chemical structure parameters given in Table I, with $\sigma = 0$ assumed for all interfaces. To avoid confusion, we stress that all fifteen Gd layers in this model have $\mathbf{m}(z)$ of identical shape, except in the top layer for which $\mathbf{m}_1(z) = 0$, with $\mathbf{m}_2(z) = (1/2)\mathbf{m}_j(z)$ for $j = 3-15$ at all z .

Figure 5 shows $m_{\parallel}(z)$ and $m_{\perp}(z)$ in histograms of S_p^{\parallel} and S_p^{\perp} , scaled magnetizations for sublayer p . For the scaling factor, see ref. 13. We divided a 4.85-nm-thick Gd layer into thirty-six sublayers of equal thickness. The Fe/Gd interfaces are located at the outer boundaries of columns $p = 1$ and 36. The molecular field of the Fe layers induces magnetizations in the Gd layers through the antiferromagnetic Fe-Gd exchange coupling, which are maximum at the interfaces and decay towards the cores of the Gd layers. To take this into account, we assumed, in ref. 13, a symmetric profile $a + b[\exp(-p/\tau) + \exp\{-(36-p)/\tau\}]$ for S_p^{\parallel} and S_p^{\perp} , where the first and second terms represent spontaneous and induced

magnetizations, respectively. We employ the same model here. b is nonzero in S_p^{\parallel} and/or S_p^{\perp} in the temperature range studied here, which is well below the Curie temperature of Fe ($T_c = 1043$ K for bulk *bcc* Fe). We determined parameters a , b , and τ so that the calculated $(I^+ - I^-)/(I^+ + I^-)_{\text{Bragg}}$ profiles agree with the observed ones individually. The negative S_p^{\parallel} values in Fig. 5 indicate in-line Gd magnetization components directed antiparallel to the applied field. The profiles for $T = 300$ K show that the cores of the Gd layers are paramagnetic with no spontaneous magnetization. We only see the induced negative S_p^{\parallel} at the Fe interfaces. Clearly, the $[\text{Fe}/\text{Gd}]_{15}$ multilayer is in the Fe-aligned state at 300 K, with the Fe and induced Gd moments directed parallel and antiparallel to the applied field, respectively, at $H = 0.5$ and 5 kOe. When cooled to 150 K, the Gd layers become ferromagnetic ($T_c \approx 210$ K; see §1), keeping the in-line magnetizations antiparallel to the field. On further cooling, S_p^{\parallel} changes the sign between $T = 150$ and 100 K at $H = 0.5$ kOe (Fig. 5A) and between 100 and 10 K at $H = 5$ kOe (Fig. 5B). The in-line components of the Gd moments switch the direction from antiparallel to parallel. As for the perpendicular components, we note $S_p^{\perp} \approx 0$ at $T \leq 100$ K in Fig. 5A(b) for $H = 0.5$ kOe except in sublayers close to the Fe interfaces. In contrast, we see finite S_p^{\perp} throughout the Gd layer at $T \leq 150$ K in Fig. 5B(b) for $H = 5$ kOe. The agreement of the calculated profiles with the data for the $\phi = 90^\circ$ configuration [Figs. 3A(b) and 3B(b)] is generally good, even though it is not as good as in Figs. 3A(a) and 3B(a).

Three-dimensional representations of $\mathbf{m}(z)$ show growing spontaneous Gd magnetizations in the layer cores with decreasing temperature (Fig. 6). On the other hand, the size of the induced Gd magnetizations at the Fe interfaces is virtually independent of temperature and external-field strength. Surprisingly, the induced magnetizations almost disappear at $T \leq 100$ K in Fig. 6B, while in Fig. 6A they are large at temperatures down to $T = 10$ K. Figure 6 illustrates how the spontaneous and induced magnetizations perform in-plane rotations as a function of temperature for the field strengths of $H = 0.5$ kOe (Fig. 6A) and 5 kOe (Fig. 6B). At $T = 150$ and 100 K, the canting angles of the induced moments markedly differ from those of the core moments. At $H = 5$ kOe, the core moments are in the nine-o'clock position from the applied-field direction when viewed from the top surface. We believe that the sign of twist angle ψ is determined by the small transverse field of the permanent magnet.¹³⁾ This is to say that when twisting is to occur by the competition of the Zeeman energy and the exchange interaction energy, the Fe–Gd moment pairs rotate either clockwise or anticlockwise with an equal probability unless biased by the transverse field. The transverse field also explains the small Bragg peaks observed in the $\phi = 90^\circ$ configuration at $T = 300$ K [Figs. 3A(b) and 3B(b)].

At $H = 0.5$ kOe, the core Gd moments are slightly twisted at $T = 150$ K, which become parallel to the applied field at $T \leq 100$ K to form the Gd-aligned structure at $T = 10$ K (Fig. 6A). This is contrasted by the case of $H = 5$ kOe, in which the Gd magnetizations are twisted once the Gd layers become ferromagnetic ($T_c \approx 210$ K) and are never parallel to the field. The missing large interface magnetization at $T \leq 100$ K (Fig. 6B) deserves a special discussion.

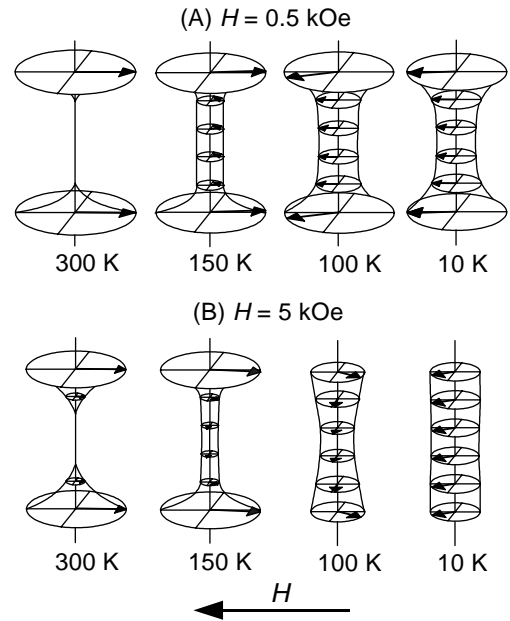


Fig. 6. 3D representations of the magnetic structures of the Gd layers in the $[\text{Fe}/\text{Gd}]_{15}$ multilayer at 300, 150, 100 and 10 K, composed from Fig. 5. (A) For applied in-plane field strength $H = 0.5$ kOe and (B) for 5 kOe. Arrows show the sizes and orientations of sublayer Gd magnetization vectors. The large disks in the top and bottom levels of the ‘drums’ represent the induced magnetizations at the Fe interface. H indicates the applied in-plane field direction. The vertical axes are along the out-of-plane direction and the multilayer surface is located towards the top of the diagrams.

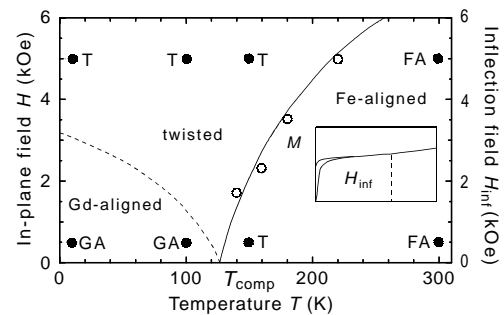


Fig. 7. Approximate magnetic phase diagram for the $[\text{Fe}/\text{Gd}]_{15}$ multilayer. The closed circles show the points at which the X-ray magnetic scattering data were collected. FA: Fe-aligned state, T: twisted state, and GA: Gd-aligned state. The open circles are the plots of the inflection fields H_{inf} observed in the $M(H)$ curves (inset).

4. Discussion

4.1 Phase diagram

The structure information obtained in §3 is summarized in the (H, T) phase diagram of Fig. 7, where the broken line shows an approximate phase boundary between the twisted state and the Gd-aligned state. We cannot determine the exact boundary location solely from the data represented by the closed circles. The solid line shows the Fe-align/twist phase boundary, estimated from macroscopic magnetization measurements. The open circles are the plots of inflection fields H_{inf} in the magnetization-versus-applied-field curves of the $[\text{Fe}/\text{Gd}]_{15}$ multilayer, observed at $T = 140$ – 220 K.

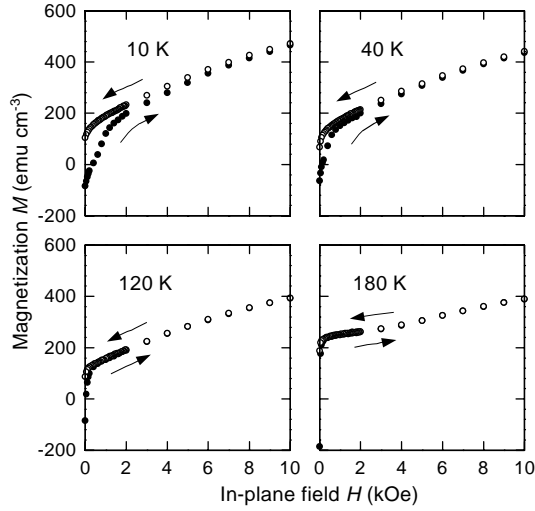


Fig. 8. Magnetization-versus-applied-field curves, $M(H)$, of the $[\text{Fe/Gd}]_{15}$ multilayer measured at $T = 10, 40, 120$ and 180 K. Data points shown by solid circles were obtained by increasing the external in-plane field $H = 0 \rightarrow 50$ kOe, whereas open circles are the data points obtained with decreasing field $H = 50 \rightarrow 0$ kOe.

The $M(H)$ curves, measured with a superconducting quantum interference device (SQUID) magnetometer, showed rapid initial increases, followed by slower rises of which the rates slightly increased beyond $H = H_{\text{inf}}$ (inset in Fig. 7; see also Fig. 8).²¹⁾ The magnetic structure derived in §3 is consistent with the expectation from the $M(H)$ curves that the $[\text{Fe}(3.5\text{ nm})/\text{Gd}(4.9\text{ nm})]_{15}$ multilayer is Fe-aligned below the solid line and twisted above, except at (0.5 kOe, 150 K).

It turns out that in Fig. 7, (5 kOe, 150 K) and (5 kOe, 100 K) are located deep in the twisted regime, where the core magnetic moments in the Gd layers are oriented perpendicular to the applied field, as pointed out in §3. Similar perpendicular Gd moments were found in our previous sample at $H = 2.4$ kOe, $T = 140$ K.¹³⁾ These moments rotate towards either the parallel or antiparallel orientation as one approaches the phase boundary, but the magnetic structures near the phase boundaries may not be simple. The small negative S_p^\perp seen at $H = 0.5$ kOe, $T = 150$ K in Fig. 5A(b) can be a manifestation of a complicated structure.

We speculate that the Gd layers in our sample include domains with easy magnetization axes broadly away from the mean magnetization direction that is parallel to the applied field in the Gd-aligned state. Energy calculations on model single-domain Gd layers demonstrate that $H^* \approx 0$ when the easy magnetization axis is perpendicular to the field, whereas $H^* \approx 5$ kOe at $T = 10$ K when the easy axis is parallel to the field, where H^* is the critical field for the Gd-align/twist phase transition.

We grew $[\text{Fe/Gd}]_{15}$ multilayers with varying Fe and Gd layer thicknesses on cooled silicon substrates at 220–150 K, some of which showed inflections in the macroscopic $M(H)$ curves measured at $T < T_{\text{comp}}$. These samples exhibit, however, fewer Bragg peaks than the one shown in Fig. 1. A weak magnetic anisotropy at low temperatures and a high multilayer order appear to be hardly compatible requirements. The sample we investigated in this paper showed no

Table II. In-line ($M_{\parallel}^{\text{Gd}}$ and $M_{\parallel}^{\text{Fe}}$) and perpendicular (M_{\perp}^{Gd}) magnetizations for the four temperatures T , calculated from the RXMS data, $\sum_p S_p^{\parallel}$ and $\sum_p S_p^{\perp}$ obtained in Fig. 5B ($H = 5$ kOe), and the measured magnetization M^{obs} for the $[\text{Fe/Gd}]_{15}$ multilayer. M^{Gd} is the magnetization size of the Gd layer. All magnetizations are in units of emu cm^{-3} (per unit volume of the $[\text{Fe/Gd}]_{15}$ multilayer).

T (K)	$\sum_p S_p^{\parallel}$	$\sum_p S_p^{\perp}$	M^{obs}	$M_{\parallel}^{\text{Gd}}$	M_{\perp}^{Gd}	M^{Gd}	$M_{\parallel}^{\text{Fe}}$
300	-23.464	0.000	408.1	-225.2	0.0	225.2	633.3
150	-23.464	13.742	284.9	-225.2	131.9	261.0	510.1
100	-11.732	37.287	289.4	-112.6	357.9	375.2	402.0
10	68.708	27.483	337.6	659.4	263.8	710.2	-321.8

hint of the Gd-align \rightarrow twist transition in the $M(H)$ curves for $T \leq T_{\text{comp}}$ (≈ 120 K), as seen in Fig. 8.

4.2 Comparison with magnetization measurement

Table II lists $\sum_p S_p^{\parallel}$ and $\sum_p S_p^{\perp}$ calculated from the magnetization maps in Fig. 5B ($H = 5$ kOe) for the four temperatures $T = 0, 50, 150$ and 300 K. An $M(H)$ curve measured at $T = 300$ K shows a magnetization $408.1 \text{ emu cm}^{-3}$ (per unit volume of the $[\text{Fe/Gd}]_{15}$ sample) at $H = 5$ kOe. This value, listed as M^{obs} in Table II, is derived with the use of $t_{\text{Fe}} = 3.53 \text{ nm}$ and $t_{\text{Gd}} = 4.85 \text{ nm}$ given in Table I. M^{obs} is the sample magnetization in line with the applied field. Assume $2.2\mu_{\text{B}}$ and $7.55\mu_{\text{B}}$ for the size of the atomic moments of Fe and Gd, respectively, and apply the layer thickness and density values in Table I to *bcc* Fe and *hcp* Gd. We then have 633.3 and $1155.8 \text{ emu cm}^{-3}$ for the saturation magnetizations of the Fe and Gd layers, M_{s}^{Fe} and M_{s}^{Gd} , respectively. The high Curie temperature of Fe assures that the Fe layers fully magnetize at all temperatures studied in this work. We can safely assume $M^{\text{Fe}} = M_{\text{s}}^{\text{Fe}}$, where M^{Fe} is the actual magnetization size of the Fe layers. At $T = 300$ K, the multilayer is in the Fe-aligned state with antiparallel Fe and Gd moments collinear with the applied field. The Gd layers should be responsible for a magnetization $M^{\text{obs}} - M^{\text{Fe}} = -225.2 \text{ emu cm}^{-3}$ in the field direction (shown under $M_{\parallel}^{\text{Gd}}$ in Table II). The negative value is consistent with the Gd moments directed opposite to the applied field. This provides a scaling factor $(M^{\text{obs}} - M^{\text{Fe}})/\sum_p S_p^{\parallel} = (-225.2)/(-23.464) = 9.589$ to calculate $M_{\parallel}^{\text{Gd}}$ and M_{\perp}^{Gd} from $\sum_p S_p^{\parallel}$ and $\sum_p S_p^{\perp}$ for the other temperatures, respectively. Here $M_{\parallel}^{\text{Gd}}$ and M_{\perp}^{Gd} are the actual in-line and perpendicular Gd magnetizations per unit volume of the multilayer, respectively. The results are indicated in the fifth and sixth columns of Table II. The magnetization size of the Gd layers, M^{Gd} , is given by $[(M_{\parallel}^{\text{Gd}})^2 + (M_{\perp}^{\text{Gd}})^2]^{1/2}$ (listed in the seventh column). The last column shows $M_{\parallel}^{\text{Fe}}$, the in-line Fe magnetizations calculated from $M_{\parallel}^{\text{Fe}} = M^{\text{obs}} - M_{\parallel}^{\text{Gd}}$ using the thus obtained $M_{\parallel}^{\text{Gd}}$ and the M^{obs} values indicated [see Fig. 8 for the $M(H)$ curves]. At $T = 300$ K, we have $M_{\parallel}^{\text{Fe}} = M^{\text{Fe}}$ since the Fe moments are parallel to the field. Note that $M_{\parallel}^{\text{Fe}}$ decreases with decreasing T in Table II. This indicates that the Fe moments rotate by an increasing angle away from the field direction. It is a good approximation to assume that the Fe layers uniformly magnetize because of the large molecular-field constant $A_{\text{Fe,Fe}}$ compared with $A_{\text{Fe,Gd}}$ and $A_{\text{Gd,Gd}}$. M^{Gd} is greater than M^{Fe} ($= 633.3 \text{ emu cm}^{-3}$) only at $T = 10$ K in Table II. In a low or moderate applied field, we expect that

$M_{\parallel}^{\text{Fe}} > 0$ and $M_{\parallel}^{\text{Gd}} < 0$ when $M^{\text{Fe}} > M^{\text{Gd}}$ and that $M_{\parallel}^{\text{Fe}} < 0$ and $M_{\parallel}^{\text{Gd}} > 0$ when $M^{\text{Fe}} < M^{\text{Gd}}$. These are preferred configurations of the antiferromagnetically coupled Fe and Gd moments: the Zeeman energy is lower than in the opposite configurations. The signs and relative magnitudes of the various M 's in Table II well match the expectation, providing evidence of the consistency of the X-ray data for $H = 5$ kOe with the macroscopic magnetization measurement. A similar but slightly degraded consistency is found in the X-ray data for $H = 0.5$ kOe.

Raw magnetization data are sensitive to trace magnetic impurities in a substrate material, which often has a volume much greater than the multilayer. This explains why we used the $[\text{Fe}/\text{Gd}]_{15}$ sample grown on a $12.5\text{-}\mu\text{m}$ -thick Kapton film for magnetization studies, instead of the $[\text{Fe}/\text{Gd}]_{15}$ on a silicon substrate. The above-described consistency of the X-ray and magnetization data is proof that the multilayers grown on the silicon and Kapton substrates have similar magnetic properties.

The X-ray data is not free from problems, however. The most serious one is the size of the Gd moments in the interface sublayers. Applying the above-derived scaling factor to the sublayers, we find $9\mu_B$ for interface Gd atoms. Another problem is the Gd magnetization at $T = 10$ K. Table II shows $M^{\text{Gd}} = 710.2\text{ emu cm}^{-3}$, which is only 60% of M_s^{Gd} , even though the Gd layers must be magnetically saturated at this low temperature. The reduced Gd magnetization is obvious in Fig. 6, where the interface sublayers have nearly full magnetizations induced by the molecular field of adjacent Fe layers. At $T = 10$ K, the radii of the 'drums' at the symmetry points (*i.e.*, layer cores) are no greater than 60–70% of those of the large disks at the top and bottom that represent the induced magnetizations. Gd magnetizations reduced by 20–30% were found previously by other groups.^{4,7,9,22,23} The deficient magnetization may be due to the multidomain structure in the Gd layers.

$M_{\parallel}^{\text{Fe}} = -321.8\text{ emu cm}^{-3}$ for $T = 10$ K in Table II, when $M^{\text{Fe}} = 633.3\text{ emu cm}^{-3}$, suggests that the Fe moments form $\pm 120^\circ$ angles with the applied-field direction, *i.e.*, $|\cos \psi| \approx 0.5$. In view of the orientation of the Gd moments in Fig. 6B, we infer that the Fe and Gd moments are nearly antiparallel at (5 kOe, 10 K). This is an energetically favored configuration of the antiferromagnetically coupled Fe and Gd moments at the interfaces. A resonant X-ray magnetic scattering experiment at the Fe edge would enable verification of this inference.

The $M(H)$ curves recorded at $T \leq 100$ K show significant hysteresis in low- H regions (see Fig. 8), indicative of the magnetic anisotropy of the Gd layers. Correspondingly, we observed distinct X-ray magnetic scattering profiles on increasing T and decreasing T . The data in Fig. 3 were collected from the sample cooled in a fixed field of the permanent magnet, which would have the stable structures of low Zeeman energy, accomplished by decreasing H at fixed T . Figure 9 shows the temperature variations of sample magnetization $M(T)$ for $H = 0.5$ and 5 kOe, derived from the $M(H)$ curves measured at various temperatures including those shown in Fig. 8. Magnetizations observed with increasing H ($0 \rightarrow 50$ kOe: H_{up}) and decreasing H ($50 \rightarrow 0$ kOe: H_{down}) are shown by solid and open symbols, respectively. The distinct magnetizations for H_{up} and H_{down} ,

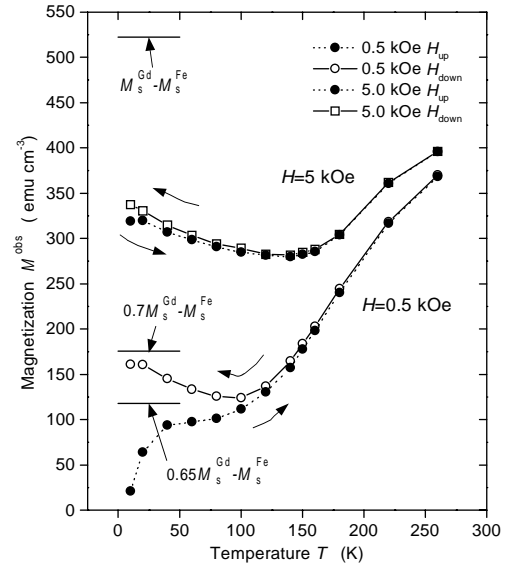


Fig. 9. $M(T)$ curves for $H = 0.5$ (circles) and 5 kOe (squares) derived from the $M(H)$ curves measured at various temperatures. Solid symbols: data points obtained from the $M(H)$ curves measured by increasing the external in-plane field $H = 0 \rightarrow 50$ kOe (H_{up}), open symbols: data points obtained from those measured with decreasing field $H = 50 \rightarrow 0$ kOe (H_{down}). The three short horizontal lines indicate the calculated magnetization levels for $M_s^{\text{Gd}} - M_s^{\text{Fe}}$, $0.7M_s^{\text{Gd}} - M_s^{\text{Fe}}$ and $0.65M_s^{\text{Gd}} - M_s^{\text{Fe}}$, where M_s^{Gd} and M_s^{Fe} are the saturation magnetizations for the Gd and Fe layers, respectively.

which are pronounced at $T \leq 100$ K for $H = 0.5$ kOe in Fig. 9, are due to the magnetic anisotropy of the Gd layers.

Support for the distinctive magnetic structures at (0.5 kOe, 10 K) and (5 kOe, 10 K) is found in the macroscopic magnetization data. Figure 9 shows $M^{\text{obs}} = 161.0\text{ emu cm}^{-3}$ at $H_{\text{down}} = 0.5$ kOe, which is close to $0.7M_s^{\text{Gd}} - M_s^{\text{Fe}}$ ($= 175.8\text{ emu cm}^{-3}$). The factor 0.7 is of the same nature as discussed above. Similarly, $M^{\text{obs}} = 337.6\text{ emu cm}^{-3}$ at $H_{\text{down}} = 5$ kOe, which is twice as large as the value at $H = 0.5$ kOe. This suggests that the multilayer is not in the same state at (0.5 kOe, 10 K) and (5 kOe, 10 K).

4.3 Magnetic structure of the Gd-aligned state

Spin configurations in polycrystalline Fe/Gd multilayers can be complicated ones at low temperatures, where Gd layers show significant magnetic anisotropy. Let the local moment of a Gd magnetic domain be $\mathbf{m}^{\text{Gd}}(z)$, of which orientation may vary from one domain to another. One may average such $\mathbf{m}^{\text{Gd}}(z)$'s at each depth level z to consider mean vector $\bar{\mathbf{m}}^{\text{Gd}}(z)$. The Gd-aligned state is defined when $\bar{\mathbf{m}}^{\text{Gd}}(z)$ has no component perpendicular to the applied field, *i.e.*, $\bar{m}_{\perp}^{\text{Gd}}(z) = 0$ at all z . This is the original notion of the Gd-aligned state.^{1–3} Alternatively, one may extend the original notion to define the Gd-aligned state when the orientation of $\bar{\mathbf{m}}^{\text{Gd}}(z)$ is independent of z , *i.e.*, $\bar{m}_{\perp}^{\text{Gd}}(z)/\bar{m}_{\parallel}^{\text{Gd}}(z) = \text{constant}$. In the second definition, the Gd-aligned state does not require the common $\bar{\mathbf{m}}^{\text{Gd}}(z)$ direction to be parallel to the external applied field. This is a twisted state according to the original definition by Camley and others,^{1–3} which presumes isotropic Gd layers. The first definition of the Gd-aligned state may apply to Fe/Gd multilayers of random anisotropy, whereas the Gd-aligned state of the second definition can be produced in Fe/Gd multilayers with

uniaxial anisotropy. In either definition, judgement between the Gd-aligned and twisted states requires information on perpendicular magnetization $\bar{m}_{\perp}^{\text{Gd}}(z)$, which cannot be known in macroscopic magnetization measurements. Our sample shows $M^{\text{obs}} \approx 0.7M_s^{\text{Gd}} - M_s^{\text{Fe}}$ at $H = 0.5$ kOe and $T = 10$ K in Fig. 9. Is this a Gd-aligned state of the first definition, $\int_0^{t_{\text{Gd}}} \bar{m}^{\text{Gd}}(z) dz \approx 0.7M_s^{\text{Gd}}$ and $\bar{m}_{\perp}^{\text{Gd}}(z) = 0$, or the one of the second definition, $\int_0^{t_{\text{Gd}}} \bar{m}^{\text{Gd}}(z) dz < M_s^{\text{Gd}}$ and $\bar{m}_{\perp}^{\text{Gd}}(z) \neq 0$? We have put $\bar{m}^{\text{Gd}} = |\bar{\mathbf{m}}^{\text{Gd}}|$ here. The X-ray results in Figs. 5 and 6 show that our Fe/Gd sample is in the Gd-aligned state of the first definition at $H = 0.5$ kOe, $T = 10$ K.

Macroscopic magnetization measurements for Fe/Gd samples provide no direct information on the perpendicular components of Fe and Gd magnetizations. This is also the case with XMCD measurements even though XMCD can separately probe the parallel magnetizations of Fe and Gd layers by tuning the X-ray energy close to the absorption edges. Our Fe/Gd multilayer shows a large increase in magnetization when the external field H is increased from 0.5 to 5 kOe at $T = 10$ K (Fig. 9). With this observation only, one cannot tell whether the increased magnetization is due to a transition from the Gd-aligned state to the twisted state, with a concomitant increase in $M_{\parallel}^{\text{Fe}}$, of the first definition or the sample remains Gd-aligned at $H = 0.5$ and 5 kOe, but with varied $\int_0^{t_{\text{Gd}}} \bar{m}^{\text{Gd}}(z) dz$. The X-ray results in Figs. 5 and 6 clearly show that the former is the case in our sample.

4.4 Induced magnetization, surface oxidation and interface roughness

The virtual disappearance of induced interface Gd magnetizations at $H = 5$ kOe, $T \leq 100$ K (Fig. 6B) is not well understood. It may be a combined effect of the domain structure and the magnetic anisotropy of the Gd layers. We suspect alternatively interface magnetic roughness, which may depend upon the bulk magnetization of the Gd layers and somehow decrease the induced magnetizations.

We assumed a 50% Fe–50% O composition for the surface oxide layer in our sample. ^{57}Fe Mössbauer studies^{15,24)} report, however, that the hyperfine field around Fe nuclei in naturally formed surface oxides on Fe films is close to the one in bulk $\gamma\text{-Fe}_2\text{O}_3$. We assumed the $\gamma\text{-Fe}_2\text{O}_3$ composition for the oxide layer in our sample, but the fit in Fig. 1 marginally improved. The oxidation of the top Fe layer somehow affected the magnetizations of the top and second Gd layers in our sample. The origin of the magnetically dead surface Gd layers remains to be elucidated.

The effect of interface roughness on X-ray reflectivity profiles is to add an extra decay term $\exp(-\sigma^2 q_z^2)$. We have two relevant σ 's in the resonant magnetic scattering, σ_{ee} and σ_{me} . The former affects the charge scattering $I^+ + I^-$, while the latter influences the magnetic-charge interference scattering $I^+ - I^-$. Recent X-ray magnetic diffuse-scattering experiments show that the charge and magnetic interfaces in multilayers have distinct roughness structures.^{25–28)} All simulations of X-ray magnetic reflectivity profiles in this work postulate ideally smooth interfaces, i.e., $\sigma_{\text{ee}} = \sigma_{\text{me}} = 0$. Even though this assumption may be justified at small q_z , a formulation of X-ray magnetic reflectivity from multilayers with rough interfaces is required for further studies.

5. Concluding Remarks

Using the element-specific RXMS technique, we have determined the magnetic structures of the Gd layers in an Fe/Gd multilayer at low temperatures, providing evidence for the first time that the Gd moments line up with the applied in-plane field everywhere in the films at $H = 0.5$ kOe, $T = 10$ K. This transforms into twisted structures with increasing H and/or T . The quality of our X-ray data is not sufficiently high to allow us to determine which of the so-called surface-twisted model and the bulk-twisted model^{1–3)} better fits the data for $H = 5$ kOe, $T = 10$ K. We have shown that the induced large Gd moments at the Fe interfaces show markedly different in-plane canting angles from the core moments, suggesting the constraint by the Fe moments through the Fe–Gd exchange coupling.²⁹⁾ It should be noted that this type of magnetic structure cannot be derived using the molecular-field theory. Our X-ray data is consistent with the macroscopic magnetization measurement, which enabled the sizes of local moments to be placed on the absolute scale. A simplified single-domain model fits the X-ray data quite well. Multidomain models and an explicit inclusion of the magnetic anisotropy of the Gd layers would improve the fit, providing information on the unexplained or not well explained aspects of the structures described in this paper, such as the disappearance of the induced interface Gd magnetizations and the unphysically large interface Gd moments. The resonant X-ray magnetic scattering at the L_3 edge probes the magnetism of the Gd $5d$ band via the electric dipole transition $2p_{3/2} \rightarrow 5d$ of core electrons. The spin polarization of the $5d$ band is induced by the strongly polarized $4f$ band through the $4f$ – $5d$ exchange coupling. It is unclear whether or not we can generally discuss the $4f$ magnetism in terms of the $5d$ magnetism, but the present work shows that the $5d$ polarization well represents the magnetization of the Gd layers in the Fe/Gd multilayer. Finally, resonant X-ray magnetic scattering experiments at the Fe K edge will explore the magnetic structures of the Fe layers, which would tell the other half of the story, allowing us to see the whole picture. Clearly, this type of experiment is not feasible with element-nonspecific neutron scattering.

Acknowledgement

We appreciate assistance by C. K. Venkataraman, C. S. Nelson, and J. C. Lang in the magnetic X-ray data collection. This work is supported by Ministry of Education, Science and Culture Grant-in-Aids, Nos. 09305019, 10044071, and 10130101 and by Japan–Korea Cooperative Science Program organized by JSPS and KOSEF. N. H. and H. H. thank Collaborative Research Projects of the Materials and Structure Laboratory, Tokyo Institute of Technology, for support. The work at the APS is supported by US-DOE-BES under Contract No. W31-109-ENG-38.

- 1) R. E. Camley: Phys. Rev. B **35** (1987) 3608.
- 2) R. E. Camley and D. R. Tilley: Phys. Rev. B **37** (1988) 3413.
- 3) J. Lepage and R. E. Camley: Phys. Rev. Lett. **65** (1990) 1152.
- 4) K. Takanashi, Y. Kamiguchi, H. Fujimori and M. Motokawa: J. Phys. Soc. Jpn. **61** (1992) 3721.
- 5) K. Cherifi, C. Dufour, G. Marchal, Ph. Mangin and J. Hubsch: J.

- Magn. Magn. Mater. **104–107** (1992) 1833.
- 6) M. Vaezzadeh, B. George and G. Marchal: Phys. Rev. B **50** (1994) 6113.
 - 7) M. Sajjeddine, Ph. Bauer, K. Cherifi, C. Dufour, G. Marchal and R. E. Camley: Phys. Rev. B **49** (1994) 8815.
 - 8) C. Dufour, K. Cherifi, G. Marchal, Ph. Mangin and M. Hennion: Phys. Rev. B **47** (1993) 14572.
 - 9) W. Hahn, M. Loewenhaupt, Y. Y. Huang, G. P. Felcher and S. S. P. Parkin: Phys. Rev. B **52** (1995) 16041.
 - 10) F. Itoh, M. Nakamura, H. Sakurai, H. Kiriake, M. Nawate, S. Honda and H. Kawata: *Proc. 7th Int. Conf. X-Ray Absorption Fine Structure*, Jpn. J. Appl. Phys. **32** (1993) Suppl. 32-2, p. 326.
 - 11) F. Itoh, M. Nakamura and H. Sakurai: J. Magn. Magn. Mater. **126** (1993) 361.
 - 12) A. Koizumi, M. Takagaki, M. Suzuki, N. Kawamura and N. Sakai: Phys. Rev. B **61** (2000) R14909.
 - 13) N. Ishimatsu, H. Hashizume, S. Hamada, N. Hosoito, C. S. Nelson, C. T. Venkataraman, G. Srarjer and J. C. Lang: Phys. Rev. B **60** (1999) 9596.
 - 14) H. Hashizume, N. Ishimatsu, O. Sakata, T. Iizuka, N. Hosoito, K. Namikawa, T. Iwazumi, G. Srarjer, C. T. Venkataraman, J. C. Lang, C. S. Nelson and L. E. Berman: Physica B **248** (1998) 133.
 - 15) T. Shinjo, T. Iwasaki, T. Shigematsu and T. Takada: Jpn. J. Appl. Phys. **23** (1984) 283.
 - 16) Alternatively, one can define $I^+(I^-)$ for the scattering intensity measured with probing X-rays of $+1(-1)$ helicity. For this definition to be meaningful, however, the applied-field orientation has to be specified. We write i^+ and i^- for the scattering intensities defined in terms of helicity only.
 - 17) More accurately, $I^+(q_z) - I^-(q_z)$ is proportional to the magnetization component parallel to $\mathbf{k} + \mathbf{k}' \cos 2\theta$ (see ref. 13). This vector is contained in the dispersion plane and is nearly parallel to the reflecting surface at small 2θ in the specular reflection geometry. For in-plane magnetizations, namely for magnetic moments parallel to the sample surface, $I^+(q_z) - I^-(q_z)$ is only sensitive to the magnetization components parallel to the dispersion plane. At small 2θ , $I^+(q_z) - I^-(q_z)$ has no sensitivity to magnetization components parallel to the surface normal.
 - 18) S. W. Lovesey and S. P. Collins: *X-ray Scattering and Absorption by Magnetic Materials* (Clarendon Press, Oxford, 1996) Chap. 6, p. 223.
 - 19) This is to say that $i^+ - i^-$ (see ref. 16) changed the sign, with the amplitude unchanged within 10%, upon a reversal of the field direction. Let us write $I^{\nu H}$ for the scattering intensity measured with X-rays of helicity ν and H field applied on the sample, where $\nu = +1$ or -1 and $H = +$ or $-$. For the $+$ field $I^+ - I^- = I^{+1+} - I^{-1+}$ and $i^+ - i^- = I^{+1+} - I^{-1+}$, and for the $-$ field $I^+ - I^- = I^{-1-} - I^{+1-}$ and $i^+ - i^- = I^{+1-} - I^{-1-}$. As the change of sign in ν is equivalent to that in H (see below), $I^+ - I^-$ does not change its sign before and after the field reversal, but $i^+ - i^-$ changes its sign. This is true, however, only if all magnetic moments in the sample become oppositely directed upon field reversal. In samples with strong magnetic anisotropy, all moments do not necessarily reverse the directions when the reversing field is low in strength. This explains the preferred use of the helicity-flip technique over the field reversal in magnetic scattering (and spectroscopy) experiments where low fields are applied on the sample.
 - 20) We write $I^+ = I_{ee} + I_{me}$, where I_{ee} and I_{me} are the charge-scattering intensity and the resonant magnetic-charge interference scattering intensity, respectively. Then $I^- = I_{ee} - I_{me}$ and $I^+ - I^- = 2I_{me}$ in the dipole-transition approximation. I_{me}/I_{ee} is a few percents at the Gd L_3 edge, as seen in Fig. 3. If I^+ and/or I^- include experimental artifacts greater than a few parts in 10^3 , the two $(I^+ - I^-)$'s measured before and after a reversal of the applied-field direction do not agree within 10%.
 - 21) In a simplified theoretical model, this behavior is explained as follows. The Gd moments remain antiparallel to the applied field up to $H = H_{inf}$, beyond which they rotate towards the field direction. So far as Gd moments are in line with the field, there is practically no increase in parallel magnetization and the $M(H)$ curve remains stationary. Once the Gd moments start rotating and leave the antiparallel orientation, the magnetization along the field direction increases and the $M(H)$ curve rises. The Fe moments do not contribute much to the magnetization along the field since they hardly change their orientations because of the strong exchange coupling: the molecular-field constant $A_{Fe,Fe}$ is much larger in value than $A_{Gd,Gd}$ and $A_{Fe,Gd}$. The size of atomic moments in ferromagnets is fixed by the molecular field and is not increased by the applied field, because the molecular field is much stronger than the applied field used in the present work.
 - 22) R. E. Camley and R. L. Stamp: J. Phys.: Condens. Matter **5** (1993) 3727.
 - 23) C. Dufour, Ph. Bauer, M. Sajjeddine, K. Cherifi, G. Marchal, Ph. Mangin and R. E. Camley: J. Magn. Magn. Mater. **121** (1993) 300.
 - 24) T. Shinjo, T. Shigematsu, N. Hosoito, T. Iwasaki and T. Takada: Jpn. J. Appl. Phys. **21** (1982) L220.
 - 25) J. F. MacKay, C. Teichert, D. E. Savage and M. G. Lagally: Phys. Rev. Lett. **77** (1996) 3925.
 - 26) J. W. Freeland, V. Chakarian, K. Bussmann, Y. U. Idzerda, H. Wende and C. C. Kao: J. Appl. Phys. **83** (1998) 6290.
 - 27) C. S. Nelson, G. Srarjer, J. C. Lang, C. T. Venkataraman, S. K. Sinha, H. Hashizume, N. Ishimatsu and N. Hosoito: Phys. Rev. B **60** (1999) 12234.
 - 28) H. Hashizume, S. Miya, T. Tanaka, N. Ishimatsu, Y. Yamaguchi, N. Hosoito, A. Sakuma and G. Srarjer: Philos. Trans. R. Soc. London A **357** (1999) 2817.
 - 29) N. Hosoito, H. Hashizume and N. Ishimatsu: submitted to J. Phys.: Condens. Matter.